CHEMISTRY OF MATERIALS
Article

Chem. Mater. **2010,** *22,* 1545–1550 1545
DOI:10.1021/cm902902j

$NaVO_2(IO_3)_2(H_2O)$: A Unique Layered Material Produces A Very Strong SHG Response

Bing-Ping Yang, Chun-Li Hu, Xiang Xu, Chuan-Fu Sun, Jian-Han Zhang, and Jiang-Gao Mao*

State Key Laboratory of Structural Chemistry, Fujian Institute of Research on the Structure of Matter, Chinese Academy of Sciences, Fuzhou 350002, P. R. China

Received September 17, 2009. Revised Manuscript Received November 26, 2009

The synthesis, crystal structure, and characterizations of a new noncentrosymmetric vanadyl iodate $NaVO_2(IO_3)_2(H_2O)$, are reported. $NaVO_2(IO_3)_2(H_2O)$ crystallizes in the polar monoclinic space group $P2_1$ (No. 4) with $a = 9.114(1)$ Å, $b = 5.2146(5)$ Å, $c = 9.216(1)$ Å, and $\beta = 111.298(8)°$. It displays a unique layered structure composed of 1D right-handed helical chains of $[(VO_2)(IO_3)_2]^-$ anions along the *b*-axis that are bridged by sodium(I) ions. The polarity in the structure is imparted by the alignment of the stereochemically active lone pairs of the iodate anions along the *b*-axis. On the basis of the powder second-harmonic generation (SHG) measurements, $NaVO_2(IO_3)_2(H_2O)$ belongs to the phase-matchable class with a very large SHG response of approximately 20 × KH_2PO_4 (KDP) or about 800 × α-quartz, which is in good agreement with the results from the theoretical calculations.

Introduction

The search of new second-order nonlinear optical (NLO) material is of current interest and great importance because of their applications in photonic technologies.[1] Currently, the explorations of second-order NLO materials used in ultraviolet and IR region are of particular research interests.[1] A few widely used second-order NLO materials used in UV, visible, and near-IR regions include KH_2PO_4 (KDP), $KTiOPO_4$ (KTP), LiB_3O_5 (LBO), β-BaB_2O_4 (BBO), α-$LiIO_3$, etc.[2] The second-order NLO materials used in the middle and far IR region are usually semiconductors based on metal chalcogenides such as $AgGaSe_2$ and metal halides such as $Cs_2Hg_3I_8$.[3] A category of "semi-organic materials", or metal-organic coordination complexes, has also been reported to show promise in the development of nonlinear optical materials.[4] As for the metal-oxide-based NLO materials, two types of cations susceptible to the second-order Jahn–Teller (SOJT) distortions, namely, octahedrally coordinated d^0 transition metal ions such as Mo^{6+}, Ti^{4+}, V^{5+}, and Nb^{5+} and cations with stereochemically active lone pairs such as I(V), Se(IV), and Te(IV), are important for the formation of noncentrosymmetric (NCS) oxides with second harmonic generation (SHG) because of the presence of the asymmetric coordination polyhedra.[5,6] Recently, we found that the combination of borates and lone pair containing Se(IV) cations can also afford new second-order NLO materials.[7] It has also been demonstrated that the combination of the above two types of SOJT distortion cations in the same compound is an effective synthetic route for new inorganic solids with excellent SHG properties if the polarizations of both types of asymmetric units are properly aligned,[8] e.g.,

*Corresponding author. FAX: (+86)591-83714946. E-mail: mjg@fjirsm.ac.cn.

(1) (a) Chen, C.; Liu, G. *Annu. Rev. Mater. Sci.* **1986**, *16*, 203. (b) Wickleder, M. S. *Chem. Rev.* **2002**, *102*, 2011.(c) Ok, K. M.; Halasyamani, P. S. Chem. Soc. Rev. **2006**, *35*, 710 and references cited therein.
(2) (a) Becker, P. *Adv. Mater.* **1998**, *10*, 979. (b) Sasaki, T.; Mori, Y.; Yoshimura, M.; Yap, Y. K.; Kamimura, T. *Mater. Sci. Eng., R* **2000**, *30*, 1. (c) Chen, C.; Lin, Z.; Wang, Z. *Appl. Phys. B: Laser Opt.* **2005**, *80*, 1–25. (d) Pan, S.; Smit, J. P.; Watkins, B.; Marvel, M. R.; Stern, C. L.; Poeppelmeier, K. R. *J. Am. Chem. Soc.* **2006**, *128*, 11631.
(3) (a) Zhang, Q.; Chung, I.; Jang, J. I.; Ketterson, J. B.; Kanatzidis, M. G. *J. Am. Chem. Soc.* **2009**, *131*, 9896. (b) Manos, M. J.; Jang, J. I.; Ketterson, J. B.; Kanatzidis, M. G. *Chem. Commun.* **2008**, 972. (c) Zhang, G.; Liu, T.; Zhu, T. X.; Qin, J. G.; Wu, Y. C.; Chen, C. T. *Opt. Mater.* **2008**, *31*, 110. (d) Zhang, G.; Qin, J. G.; Liu, T.; Zhu, T. X.; Fu, P. Z.; Wu, Y. C.; Chen, C. T. *Cryst. Growth Des.* **2008**, *8*, 2946.
(4) (a) Rivera, J. M.; Reyes, H.; Cortes, A.; Santillan, R.; Lacroix, P. G.; Lepeti, C.; Nakatani, K.; Farfan, N. *Chem. Mater.* **2006**, *18*, 1174–1183. (b) Prakash, M. J.; Radhakrishman, T. P. *Inorg. Chem.* **2006**, *45*, 9758–9764. (c) Ye, Q.; Li, Y.-H.; Song, Y.-M.; Huang, X.-F.; Xiong, R.-G.; Xue, Z.-L. *Inorg. Chem.* **2005**, *44*, 3618. (d) Bi, W.; Louvain, N.; Mercier, N.; Luc, J.; Rau, I.; Kajzar, F. *Adv. Mater.* **2008**, *20*, 1013. (e) Ye, Q.; Li, Y.-H.; Wu, Q.; Song, Y.-M.; Wang, J.-X.; Zhao, H.; Xiong, R. G.; Xue, Z. *Chem.—Eur. J.* **2005**, *11*, 988.
(5) (a) Halasyamani, P. S. *Chem. Mater.* **2004**, *16*, 3586. (b) Muller, E. A.; Cannon, R. J.; Sarjeant, A. N.; Ok, K. M.; Halasyamani, P. S.; Norquist, A. *J. Cryst. Growth Des.* **2005**, *5*, 1913.
(6) (a) Ok, K. M.; Halasyamani, P. S. *Angew. Chem., Int. Ed.* **2004**, *43*, 5489. (b) Phanon, D.; Gautier-Luneau, I. *Angew. Chem., Int. Ed.* **2007**, *46*, 8488.
(7) Kong, F.; Huang, S.-P.; Sun, Z.-M.; Mao, J.-G.; Cheng, W.-D. *J. Am. Chem. Soc.* **2006**, *128*, 7750.
(8) (a) Sykora, R. E.; Ok, K. M.; Halasyamani, P. S.; Albrecht-Schmitt, T. E. *J. Am. Chem. Soc.* **2002**, *124*, 1951. (b) Sykora, R. E.; Wells, D. M.; Albrecht-Schmitt, T. E. *Inorg. Chem.* **2002**, *41*, 2697. (c) Shehee, T. C.; Sykora, R. E.; Ok, K. M.; Halasyamani, P. S.; Albrecht-Schmitt, T. E. *Inorg. Chem.* **2003**, *42*, 457. (d) Ra, H.-S.; Ok, K.-M.; Halasyamani, P. S. *J. Am. Chem. Soc.* **2003**, *125*, 7764. (e) Chi, E. O.; Ok, K. M.; Porter, Y.; Halasyamani, P. S. *Chem. Mater.* **2006**, *18*, 2070. (f) Chang, H.-Y.; Kim, S.-H.; Halasyamani, P. S.; Ok, K. M. *J. Am. Chem. Soc.* **2009**, *131*, 2426. (g) Chang, H.-Y.; Kim, S.-H.; Ok, K. M.; Halasyamani, P. S. *J. Am. Chem. Soc.* **2009**, *131*, 6865. (h) Hu, T.; Qin, L.; Kong, F.; Zhou, Y.; Mao, J.-G. *Inorg. Chem.* **2009**, *48*, 2193. (i) Sun, C.-F.; Hu, C.-L.; Ling, J.-B.; Hu, T.; Kong, F.; Long, X.-F.; Mao, J.-G. *J. Am. Chem. Soc.* **2009**, *131*, 9486–9487.

Published on Web 01/12/2010

Table 1. Crystallographic Data for $NaVO_2(IO_3)_2(H_2O)$

compound	$NaVO_2(IO_3)_2(H_2O)$	μ, mm^{-1}	8.856
formula	$H_2I_2NaO_9V$	F(000)	428
fw	473.75	cryst size (mm^3)	0.30 × 0.20 × 0.10
temp (K)	293(2)	no. reflns collected/unique	3091/1716
space group	$P2_1$ (No. 4)	R(int)	0.0404
a (Å)	9.114(1)	completeness to θ = 27.48 (%)	98.7
b (Å)	5.2146(5)	GOF	1.013
c (Å)	9.216(1)	R_1, wR_2^{a} [$I > 2\sigma(I)$]	0.0266, 0.0545
β (deg)	111.298(8)	R_1, wR_2 (all data)	0.0296, 0.0555
V (Å^3)	408.10(9)	absolute structure param	0.02(4)
Z	2	extinction coefficient	0.0033(8)
D_{calcd} (g cm^{-3})	3.855	largest diff. peak and hole (e Å^{-3})	0.856 and −1.378

^{a} $R_1 = \sum||F_o| - |F_c||/\sum|F_o|$, $wR_2 = \{\sum w[(F_o)^2 - (F_c)^2]^2/\sum w[(F_o)^2]^2\}^{1/2}$.

$BaNbO(IO_3)_5$ displays a very large SHG response of about 14 × KDP.[8i] As for the alkali metal−V(V)−iodate system, the nonisostructural centrosymmetric $A(VO_2)(IO_3)_2$ (A = Li, K, Rb) and isostructural polar 1D $A(VO)_2(IO_3)_3(O_2)$ (A = NH_4, Rb, Cs) have been reported,[9] among which the cesium phase displays a SHG response of 500 × α-quartz.[9a] It is noted that in polar 1D $A(VO)_2(IO_3)_3(O_2)$ (A = NH_4, Rb, Cs), the polarizations of one-third of IO_3 groups cancel each other, hence the structural arrangement of the iodate groups is not optimized to produce maximum SHG efficiency. Thus far, no Na phase has been reported, it may exhibit a new structure type in-between those of lithium(I) and potassium(I) phases. Our efforts to explore the unknown Na^+−Ga^{3+}−V^{5+}−I^{5+}−O phase led to the discovery of a unique layered polar material consisting of right-handed anionic helical chains that are bridged by sodium(I) cations, namely, $NaVO_2(IO_3)_2(H_2O)$, in which the polarizations of all of the iodate groups are aligned in the same direction to produce a very large SHG response of about 20 × KDP (KH_2PO_4) (or about 800 × α-quartz). Herein we report its synthesis, crystal structure, and second-order NLO properties.

Experimental Section

Materials and Methods. All of the chemicals were analytically pure from commercial sources and used without further purification. $NaVO_3\cdot 2H_2O$ (≥98%), Ga_2O_3 (≥99.9), and I_2O_5 (≥99%) were purchased from the Shanghai Reagent Factory. Microprobe elemental analyses were performed on a field-emission scanning electron microscope (FESEM, JSM6700F) equipped with an energy-dispersive X-ray spectroscope (EDS, Oxford INCA). The X-ray powder diffraction data were collected on a Panalytical X'pert Pro MPD diffractometer using graphite-monochromated Cu−Ka radiation in the 2θ range of 5−70° with a step size of 0.02°. TGA and DTA studies were all carried out with a NETZSCH STA 449C instruments. The sample and reference (Al_2O_3) were enclosed in a platinum crucible and heated at a rate of 10 °C/min from room temperature to 1000 °C under a nitrogen atmosphere. The IR spectrum was recorded on a Magna 750 FT-IR spectrometer as KBr pellets in the range of 4000−400 cm^{-1}. The UV−vis absorption and optical diffuse reflectance spectrum was measured at room temperature with a PE Lambda 900 UV−vis spectrophotometer in the range of 2500−200 nm. $BaSO_4$ plate was used as a standard (100% reflectance). The absorption spectrum was calculated from reflectance spectrum using the Kubelka−Munk function:[10] $\alpha/S = (1 - R)^2/2R$, where α is the absorption coefficient, S is the scattering coefficient that is practically wavelength independent when the particle size is larger than 5 μm, and R is the reflectance. The measurements of the powder frequency-doubling effects were carried out by means of the method of Kurtz and Perry.[11] A 1064 nm radiation generated by a Q-switched Nd: YAG solid-state laser was used as the fundamental frequency light. The sample was ground and sieved into several distinct particle size ranges (0−25, 25−44, 44−53, 53−74, 74−105, 105−149, 149−210, 210−250 μm). Samples of KDP were prepared as reference materials in identical fashion to assume the SHG effect.

Preparations of $NaVO_2(IO_3)_2(H_2O)$. Single crystals of $NaVO_2(IO_3)_2(H_2O)$ were synthesized by the hydrothermal reactions of a mixture of $NaVO_3\cdot 2H_2O$ (1 mmol, 158 mg), Ga_2O_3 (0.25 mmol, 46.9 mg), I_2O_5 (3 mmol, 1.00 g) and 5 mL of water sealed in an autoclave equipped with a Teflon linear (23 mL) at 200 °C for 4 days, and then cooled to 30 at 6 °C/h. The final reaction product was washed with water and ethanol, and then dried in air. Light yellow hexagonal-shaped single crystals of $NaVO_2(IO_3)_2(H_2O)$ were collected in a ca. 83% yield based on V. When the reactions were carried out in absence of Ga_2O_3, only V_2O_5 powder (XRD PDF#78−2265) was isolated. It is still not clear what role Ga_2O_3 played in the formation of $NaVO_2(IO_3)_2(H_2O)$.

Single-Crystal Structure Determination. A light yellow hexagonal-shaped single crystal (dimensions 0.3 × 0.2 × 0.1 mm^3) was glued on to a glass fiber and data were collected on a SCXmini CCD diffractometer equipped with a graphite-monochromated Mo−Kα radiation (λ = 0.71073 Å) at 293 K. The data sets were corrected for Lorentz and polarization factors as well as for absorption by SADABS program.[12] The structure was solved by the direct method and refined by full-matrix least-squares fitting on F^2 by SHELX-98.[12] All non-hydrogen atoms were refined with anisotropic thermal parameters. Hydrogen atoms associated with aqua ligands were located at geometrically calculated positions and refined with isotropic thermal parameters. Crystallographic data and structural refinements for the compound are summarized in Table 1. Important bond lengths are listed in Table 2. More details on the crystallographic studies as well as atom displacement parameters are given in the Supporting Information.

Theoretical Basis. Single-crystal data were used for the electronic and optical properties calculations. All calculations were

(9) (a) Sykora, R. E.; Ok, K. M.; Halasyamani, P. S.; Wells, D. M.; Albrecht-Schmitt, T. E. *Chem. Mater.* **2002**, *14*, 2741–2749. (b) Chen, X. A.; Zhang, L.; Chang, X. A.; Zang, H. G.; Xiao, W. Q. *Acta Crystallogr.* **2006**, *C62*, i76.
(10) Kubelka, P.; Munk, F. Z. *Tech. Phys.* **1931**, *12*, 593.
(11) Kurtz, S. W.; Perry, T. T. *J. Appl. Phys.* **1968**, *39*, 3798.
(12) Sheldrick, G. M. *SHELXTL Crystallographic Software Package*, version 5.1; Bruker-AXS: Madison, WI, 1998.

Table 2. Selected Bond Lengths (Å) for $NaVO_2(IO_3)_2(H_2O)^a$

Na(1)−O(1W)	2.385(7)	I(1)−O(3)	1.773(6)	V(1)−O(7)	1.618(6)
Na(1)−O(7)#1	2.414(7)	I(1)−O(1)	1.835(5)	V(1)−O(8)	1.640(5)
Na(1)−O(1)#2	2.419(6)	I(1)−O(2)	1.851(5)	V(1)−O(6)	1.970(6)
Na(1)−O(5)	2.431(7)	I(2)−O(4)	1.782(6)	V(1)−O(1)#3	2.014(5)
Na(1)−O(8)	2.485(6)	I(2)−O(5)	1.803(5)	V(1)−O(2)	2.038(5)
Na(1)−O(7)	2.587(7)	I(2)−O(6)	1.873(5)		
Na(1)−O(3)#2	2.931(7)				

[a] Symmetry transformations used to generate equivalent atoms: #1 $-x+2, y-1/2, -z+2$; #2 $x+1, y, z$; #3 $-x+1, y-1/2, -z+2$.

carried out by using the total-energy code of CASTEP.[13] The total energy was calculated within the framework of nonlocal gradient-corrected approximations (Perdew−Burke−Ernzerhof (PBE) functional).[14] The interactions between the ionic cores and the electrons was described by the norm-conserving pseudopotential.[15] The following orbital electrons were treated as valence electrons: Na-$2s^22p^63s^1$, V-$3d^34s^2$, I-$5s^25p^5$, O-$2s^22p^4$, and H-$1s^1$. The number of plane waves included in the basis was determined by a cutoff energy of 700 eV, and the numerical integration of the Brillouin zone was performed using a $3 \times 5 \times 3$ Monkhorst-Pack k-point sampling. It is important to include a significant number of empty bands when calculating optical properties, and more than 160 empty bands were used in our calculations of optical properties.

The calculations of linear optical properties in terms of the complex dielectric function $\varepsilon(\omega) = \varepsilon_1(\omega) + i\varepsilon_2(\omega)$ were made. The imaginary part of the dielectric function ε_2 was given in the following equation[16]

$$\varepsilon_2^{ij}(\omega) = \frac{8\pi^2\hbar^2e^2}{m^2V}\sum_k\sum_{cv}(f_c - f_v)\frac{p_{cv}^i(k)p_{vc}^j(k)}{E_{vc}^2}\delta[E_c(k) - E_v(k) - \hbar\omega] \quad (1)$$

f_c and f_v represent the Fermi distribution functions of the conduction and valence bands, respectively. The term $p_{cv}^i(k)$ denotes the momentum matrix element transition from the energy level c of the conduction band to the level v of the valence band at a certain k point in the Brillouin zones and V is the volume of the unit cell. m, e, and $\hbar$ are the electron mass, charge, and Plank's constant, respectively.

The first-order susceptibility and linear refractive index can be derived from the dielectric function. The first-order nonresonance susceptibility at low frequency region is given by $\chi^{(1)}(\omega)_{ii} = [\varepsilon(\omega)_{ii} - 1]/4\pi$, and the second-order susceptibilities can be expressed in terms of the first-order susceptibilities as follows[17]

$$\chi_{ijk}^{(2)}(-\omega_3;\omega_1,\omega_2) = F^{(2)}\chi_{ii}^{(1)}(\omega_3)\chi_{jj}^{(1)}(\omega_1)\chi_{kk}^{(1)}(\omega_2) \quad (2)$$

Where $F^{(2)} = ma/(N^2e^3)$. These expressions are derived from a classical anharmonic oscillator (AHO) model. The m and e are, respectively, the electron mass and charge, N is the density number of atoms in a crystal, and the parameter a, which characterizes the nonlinearity of the response, can be obtained from experimental or theoretical estimations.

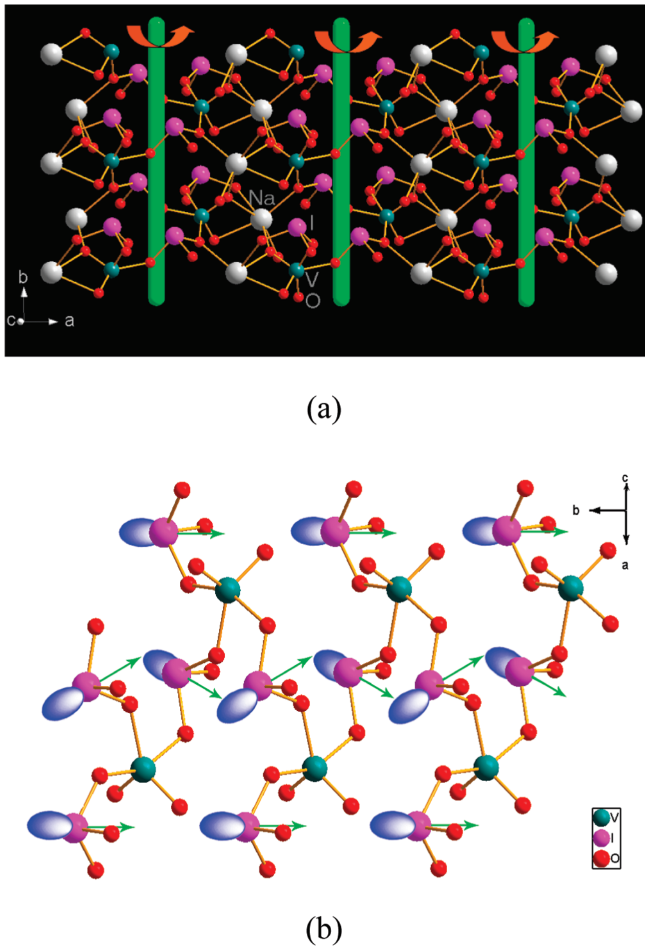

Figure 1. (a) 2D layer and (b) 1D helical anionic chain with the macroscopic polarity indicated by small green arrows in $NaVO_2(IO_3)_2$-(H_2O).

Results and Discussion

Structural Description. $NaVO_2(IO_3)_2(H_2O)$ displays a unique layered structure composed of 1D right-handed helical chains of $[(VO_2)(IO_3)_2]^-$ anions along the b-axis that are bridged by sodium(I) ions (Figure 1). The vanadium(V) cation is in a strongly distorted trigonal bipyramidal geometry, being coordinated by three oxygen atoms from three iodate groups (V−O 1.970(6)-2.038(5) Å) and two terminal oxo anions (V−O 1.618(6)-1.640(5) Å), caused by the bent nature of the O=V=O bond angle (105.8(3) °). The axial O−V−O bond angle of 152.9(2)° is significantly larger than those of the remaining ones (76.3(2)−134.2(3)°). Each I^{5+} cation is in an asymmetric coordination environment attributed to the mixing of the s- and p-orbitals of the iodine cation with p-states of the oxide anion.[5a] Both I^{5+} cations in the asymmetric unit are coordinated by three oxygen atoms in a distorted trigonal-pyramidal geometry. The I−O distances are in the range of 1.773(6)−1.873(5) Å, which are comparable to those in $A(VO_2)(IO_3)_2$ (A = Li, K, Rb).[9]

(13) (a) Segall, M. D.; Lindan, P. L. D.; Probert, M. J.; Pickard, C. J.; Hasnip, P. J.; Clark, S. J.; Payne, M. C. *J. Phys.: Condens. Matter* **2002**, *14*, 2717. (b) Milman, V.; Winkler, B.; White, J. A.; Pickard, C. J.; Payne, M. C.; Akhmatskaya, E. V.; Nobes, R. H. *Int. J. Quantum Chem.* **2000**, *77*, 895.
(14) Perdew, J. P.; Burke, K.; Ernzerhof, M. *Phys. Rev. Lett.* **1996**, *77*, 3865.
(15) Lin, J. S.; Qteish, A.; Payne, M. C.; Heine, V. *Phys. Rev.* **1993**, *B 47*, 4174.
(16) Bassani, F.; Parravicini, G. P. *Electronic States and Optical Transitions in Solids*; Pergamon Press Ltd: Oxford, U.K., 1975; pp 149−154.
(17) Boyd, R. W. In *Nonlinear Optics*; Academic Press: New York, 1992; pp 21−32.

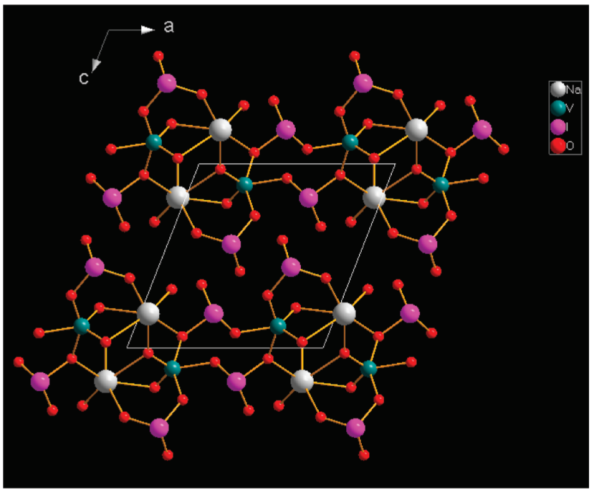

Figure 2. View of structure of $NaVO_2(IO_3)_2(H_2O)$ down the *b*-axis.

The interconnection of vanadium(V) atoms via bidentate bridging $I(1)O_3$ groups results in a unique right-handed helical chain along the *b*-axis, the $I(2)O_3$ groups are attached monodentately on both sides of the helical chain (Figure 1b). Within the 1D helical chain the V atoms are arranged in a unusual zigzag manner rather than linearly in $A(VO_2)(IO_3)_2$ (A = K, Rb) and polar 1D $A(VO)_2(IO_3)_3(O_2)$ (A = NH_4, Rb, Cs).[9] This type of anionic chain has not been observed in metal iodates. The V···V separation between the first and the third V atom of 5.215(1) Å is even much shorter than that between two neighboring ones bridged by an iodate group (5.589(1) Å). Such a strongly twisted chain allows all of the lone pairs on the IO_3^- anions are to be aligned in the same direction and produce a macroscopic dipole moment toward the $-b$ direction, which is favorable to produce a large SHG response.

Neighboring 1D helical chains are further interconnected by sodium(I) ions into a 2D layer parallel to the *ab* plane, producing a large net macroscopic dipole moment also along the $-b$ direction (Figure 1). There are very weak interlayer I···O interactions (2.772(3) Å). Each Na^+ cation is octahedrally coordinated by six oxygen atoms from an aqua ligand, two IO_3 groups in a unidentate fashion and three oxo anions with Na−O distances in the range of 2.385(7)−2.587(7) Å. Na−O(1w) bond distance of 2.385(7) Å is the shortest among the six Na−O bonds. The IO_3 groups adopt two types of coordination modes. $I(1)O_3$ is tridentate, it bridges with two V atoms (O1 and O2) and also bonds with a sodium(I) ion (O1), O3 remains noncoordinated (the very weak Na(1)−O(3) contact of 2.931(7) Å is ignored). $I(2)O_3$ group is bidentate, binding with a V atom (O6) and a sodium(I) ion (O5), the third one (O4) remains noncoordinated (Figure 2). Results of bond valence calculations indicate that Na, V and I atoms are in oxidation states of +1, +5, and +5, respectively.[18] The calculated total bond valences

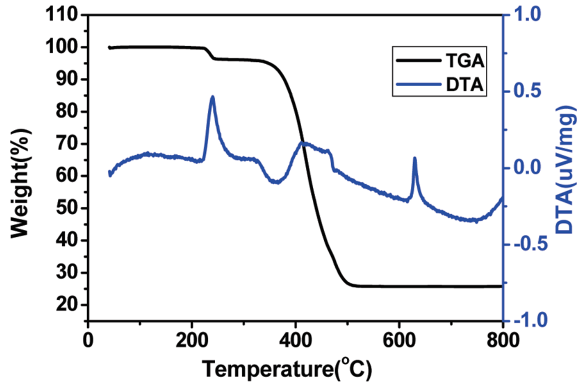

Figure 3. TGA and DTA diagrams for $NaVO_2(IO_3)_2(H_2O)$.

are 1.050, 4.934, 4.905, and 4.915 for Na(1), V(1), I(1), and I(2), respectively.

It is worth to compare the structure of $NaVO_2(IO_3)_2(H_2O)$ with those of $A(VO_2)(IO_3)_2$ (A = Li, K, Rb) and polar 1D $A(VO)_2(IO_3)_3(O_2)$ (A = NH_4, Rb, Cs).[9] $Li(VO_2)(IO_3)_2$ ($P2_1/c$) features a 2D anionic layer of $[VO_2(IO_3)_2]^-$ in which two VO_2^+ groups are bridged by a pair of iodate groups into a V_2I_2 4-MR secondary building unit (SBU), such SBUs are further bridged by additional iodate groups into a layered structure with additional V_6I_6 12-MRs.[9b] Both $K(VO_2)(IO_3)_2$ ($P2_1/n$) and $Rb(VO_2)(IO_3)_2$ ($P\bar{1}$) feature a 1D anionic chain of $[VO_2(IO_3)_2]^-$ in which neighboring V atoms are interconnected by bidentate iodate groups and the monodentate iodates groups are attached on the same side of the chain. Because all three phases crystallized in the centrosymmetric space groups, they are not SHG-active. The isostructural $A(VO)_2(IO_3)_3(O_2)$ (A = NH_4, Rb, Cs) (*Ima*2) feature a 1D chain of corner-sharing VO_6 octahedra in which each pair of V atoms are further bridged by one and two iodate groups alternatively. The polarizations of $I(2)O_3$ groups cancel each other whereas $I(1)O_3$ groups produce a macroscopic dipole moments along the *c* direction and a moderate SHG response of 500 × α-quartz was reported for the cesium compound.[9a] We speculate that the different structure for the sodium compound is probably mainly due to the different ionic size of sodium(I) as well as the presence of a strongly coordinated aqua ligand.

Thermal Stability Studies. Results of TGA studies indicate that $NaVO_2(IO_3)_2(H_2O)$ is stable up to 218 °C. Upon further heating the aqua ligand is released. Afterward the iodate groups start to decompose through thermal disproportionation which ends at 530 °C (Figure 3). These assignments are in agreement with the two endothermic peaks at 240 and 411 °C in the DTA diagram (Figure 3). After dehydration, the compound becomes amorphous but still SHG active (see Figure S1 in the Supporting Information). Hence the dehydrated species should be still structurally noncentrosymmetric. The final residual is $NaVO_3$ based on the XRD powder diffraction studies (see Figure S2 in the Supporting Information). The total weight loss of 74.31% at 600 °C matches well with the calculated value of 74.26%.

(18) (a) Brown, I. D.; Altermatt, D. *Acta Crystallogr., Sect. B* **1985**, *41*, 244. (b) Brese, N. E.; O'Keeffe, M. *Acta Crystallogr., Sect. B* **1991**, *47*, 192.

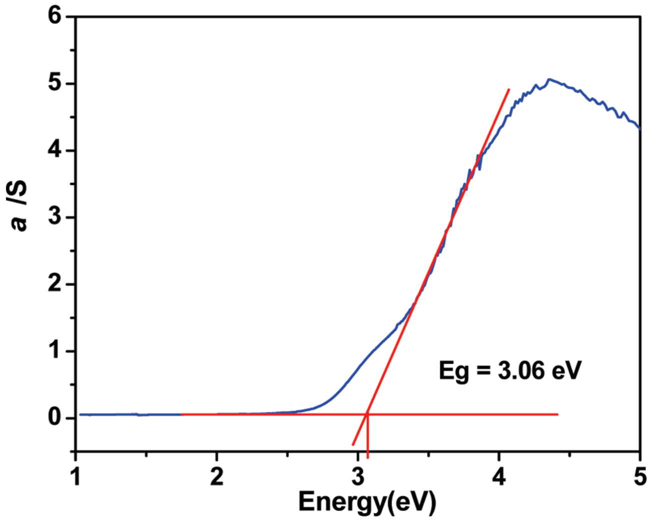

Figure 4. UV−vis diffuse reflectance spectrum for $NaVO_2(IO_3)_2(H_2O)$.

Infrared and UV−vis Absorption and Diffuse Reflectance Spectra. IR spectrum of $NaVO_2(IO_3)_2(H_2O)$ shows the characteristic absorption bands of ν_{V-O} at 914 and 952 cm^{-1}. The symmetric (ν1) and antisymmetric (ν3) IO_3^- stretching bands appear in the range 691−833 cm^{-1}, and the bands of its bending mode are observed between 463 and 506 cm^{-1}. The bands of ν_{H-O} are observed at 3416, 3239, and 1660 cm^{-1} (see Figure S3 in the Supporting Information).[9,19] Its UV−vis absorption spectrum reveals little absorption from 0.5 to 2.5 μm (see Figure S4 in the Supporting Information). Optical diffuse reflectance spectrum indicates an optical band gap of 3.06 eV, which is derived from the extrapolation of the absorption edge to the baseline; hence $NaVO_2(IO_3)_2(H_2O)$ is a wide band gap semiconductor (Figure 4).

Nonlinear Optical Properties. The polar structure of $NaVO_2(IO_3)_2(H_2O)$ prompts us to measure its second-harmonic-generation (SHG) properties. Figure 5 shows the curves of the SHG signal intensity vs particle size for ground $NaVO_2(IO_3)_2(H_2O)$ crystals. For large particle sizes, the second-harmonic intensity is independent of particle size. Features of the curves are well-consistent with phase-matching behavior according to the rule proposed by Kurtz and Perry,[11] which indicates that $NaVO_2(IO_3)_2(H_2O)$ crystal belongs to the phase-matching class. Comparison of the second-harmonic signal produced by $NaVO_2(IO_3)_2(H_2O)$ sample and KDP sample in the same particle range from 105 to 149 μm reveals that $NaVO_2(IO_3)_2(H_2O)$ exhibits a very large SHG response of about 20 × KDP (about 800 × α-quartz). The extremely large SHG efficiency should be attributed to the synergic effect of the polarizations of asymmetric IO_3^- anions within the 1D helical anionic chain, 2D layer, as well as 3D packing (Figures 1 and 2).

Theoretical Calculations. To gain further insights on the electronic structure and optical properties of $NaVO_2(IO_3)_2(H_2O)$, we performed theoretical calculations based on DFT methods by using the total-energy code CASTEP.[13]

(19) Ok, K. M.; Halasyamani, P. S. *Inorg. Chem.* **2005**, *44*, 2263.

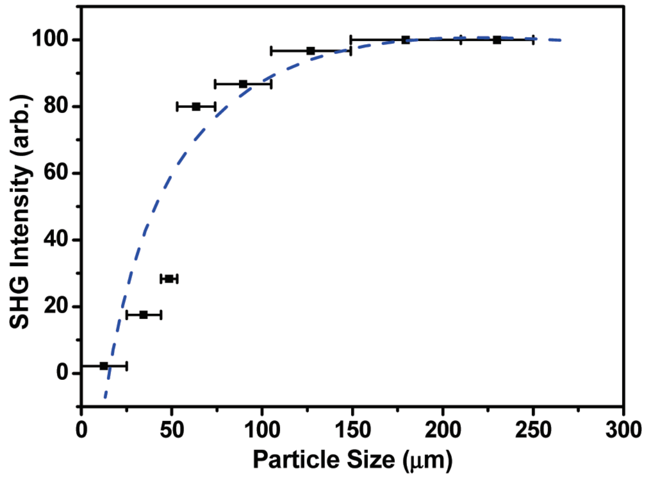

Figure 5. Phase-matching curve for $NaVO_2(IO_3)_2(H_2O)$. The curve drawn is to guide the eye and not a fit to the data.

The dispersions of energy bands are presented in Figure S5 in the Supporting Information and the density of states (DOS) is shown in Figure S6 in the Supporting Information. The top of valence bands (VB) is located at the *Z* point, and the bottom of conduction bands (CB) is located at the *B* point, hence, $NaVO_2(IO_3)_2(H_2O)$ is an indirect band gap semiconductor (see Table S1 in the Supporting Information). The calculated band gap is 2.56 eV, which is smaller than the experimental value of 3.06 eV; it is well-known that the DFT-GGA does not accurately describe the eigenvalues of the electronic states, causing the quantitative underestimation of band gaps.[20] Hence, a scissor of 0.5 eV was applied during the optical property calculations. From the DOS and PDOS diagrams (see Figure S6 in the Supporting Information), it is clear that the bands above the Fermi level are predominately derived from V-3d, O-2p, and I-5p states. The VBs from −7.6 eV to the Fermi level are also composed of O-2p, V-3d, and I-5p states. The bands from −11.7 to −7.9 eV originate mainly from O-2p, I-5s, and O-2s states. The VBs ranging from −18.5 to −14.3 eV arise from the O-2s, I-5p, and small amounts of V-3d states. The VBs ranging from −20.7 to −18.5 eV are composed of the O-2s and I-5s states. The lowest VB ranging from −22.2 to −20.7 eV arises from the Na-2p states.

The calculation and analysis of optical properties for a low-symmetry crystal should be based on the principal dielectric axis coordinate system. For the monoclinic crystal, only one dielectric axis is superposed to the *b* axis, whereas the direction of the principal dielectric axes in the *ac* plane is not related to any specific crystallographic direction. Hence the principal dielectric axes in the *ac* plane must be determined before the optical calculation.

First, in the original coordinate system (i.e., $y \parallel b$, $z \parallel c$), we calculated the optical permittivity tensor elements ε_{ij},

(20) (a) Okoye, C. M. I. *J. Phys.: Condens. Matter* **2003**, *15*, 5945. (b) Huang, S. P.; Cheng, W. D.; Wu, D. S.; Li, X. D.; Lan, Y. Z.; Li, F. F.; Shen, J.; Zhang, H.; Gong, Y. J. *J. Appl. Phys.* **2006**, *99*, 013516.

as shown below

$$\begin{bmatrix} \varepsilon_{11} & 0 & \varepsilon_{13} \\ 0 & \varepsilon_{22} & 0 \\ \varepsilon_{13} & 0 & \varepsilon_{33} \end{bmatrix} = \begin{bmatrix} 3.28997 & 0 & -0.03533 \\ 0 & 3.28889 & 0 \\ -0.03533 & 0 & 4.05921 \end{bmatrix}$$

Then, the above ε_{ij} tensor matrix was transformed to its diagonal form (i.e., the principal axes transformation), and through eq 3, the rotation angle θ between the original coordinate axes and the principal dielectric axes in the *ac* plane was calculated to be $-2.624142°$.[21]

$$tg2\theta = \frac{2\varepsilon_{13}}{\varepsilon_{33} - \varepsilon_{11}} \quad (3)$$

Finally, by the operation of rotation, the coordinate axes in the calculated structure were set to be coincident with the principal dielectric axes. The optical properties of $NaVO_2(IO_3)_2(H_2O)$, including the complex dielectric function, the refractive index, and the second-order susceptibilities were calculated in the principal dielectric axis coordinate system.

The linear optical response properties of $NaVO_2(IO_3)_2$-(H_2O) was examined through calculating the complex dielectric function $\varepsilon(\omega) = \varepsilon_1(\omega) + i\varepsilon_2(\omega)$. Its imaginary part $(\varepsilon_2(\omega))$ can be used to describe the real transitions between the occupied and unoccupied electronic states. The imaginary part of the frequency-dependent dielectric function of $NaVO_2(IO_3)_2(H_2O)$ shows anisotropy along three principal dielectric axial directions (see Figure S7 in the Supporting Information). The curves of the averaged imaginary part and real part of dielectric function were obtained by $\varepsilon^{avg} = (\varepsilon_x + \varepsilon_y + \varepsilon_z)/3$ (see Figure S7b in the Supporting Information). The averaged imaginary part reveals the strongest absorption peak at 5.26 eV, which can be mainly assigned to the electronic interband transitions from the O 2p to I 5p and V 3d states. The average static dielectric constant $\varepsilon(0)$ is 4.31. The dispersion of principal refractive index (see Figure S8 in the Supporting Information), which was calculated by the formula $n^2(\omega) = \varepsilon(\omega)$, indicates an order of $n^z > n^x > n^y$ in the low-energy range. The n^x, n^y, and n^z at 1064 nm (1.165 eV) are calculated to be 2.14, 1.99, and 2.20, respectively.

The space group of $NaVO_2(IO_3)_2(H_2O)$ belongs to class *2* and has 8 nonvanishing tensors of second-order susceptibility. Under the restriction of Kleinman's symmetry, only four independent SHG tensors (d_{14}, d_{16}, d_{22}, and d_{23}) are left. The frequency-dependent SHG tensors of $NaVO_2(IO_3)_2(H_2O)$ are plotted in Figure 6. The values of d_{14}, d_{16}, d_{22}, and d_{23} at the wavelength of 1064 nm (1.165 eV) for $NaVO_2(IO_3)_2(H_2O)$ are 2.24×10^{-8}, 2.09×10^{-8}, 1.40×10^{-8}, and 2.33×10^{-8} esu, respectively. These values are very close to our experimental value of 20 times of KDP ($d_{36} = 1.1 \times 10^{-9}$ esu).

(21) Lang, W.; Claus, R. *Phys. Rev. B* **1982**, *26*, 7119.

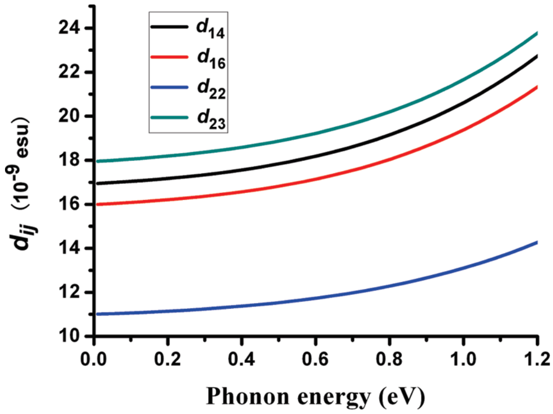

Figure 6. Calculated frequency-dependent SHG coefficients of $NaVO_2$-$(IO_3)_2(H_2O)$.

In conclusion, the electronic structures and linear and second-order nonlinear optical properties of $NaVO_2$-$(IO_3)_2(H_2O)$ have been explored theoretically. The calculated band gap is smaller than the experimental one derived from the UV−vis diffuse reflectance spectrum by 0.5 eV. The calculated SHG coefficients are in consistent with the experimental one based on the powder SHG measurements. Results of the theoretical calculations could provide some valuable information for our future studies on its bulk single crystals.

Conclusions

In summary, a new NLO material, $NaVO_2(IO_3)_2(H_2O)$, has been prepared. It features unique 1D right-handed helical chains of $[VO_2(IO_3)_2]^-$ that are further interconnected by sodium(I) ions into a 2D layer. The polarizations of all of the iodate groups are aligned along the polar axis to produce a large macroscopic dipole moment. From the second-harmonic generation (SHG) measurements on powders, $NaVO_2$-$(IO_3)_2(H_2O)$ is established to belong to phase-matchable class with a very large SHG response of approximately 20 × KH_2PO_4 (KDP), which is in good agreement with the results obtained from the theoretical calculations. On the basis of these arguments, this compound is potentially a new candidate for applications as new second−order NLO materials. Our future research efforts will be devoted to grow $NaVO_2$-$(IO_3)_2(H_2O)$ crystals with large size to further study its optical properties, such as refractive index, the Sellmeier equations, second-order NLO coefficients, and laser damage threshold.

Acknowledgment. We thank the Nation Natural Science Foundation of China (20825104, 20731006, and 20821061) and the Key Project of FJIRSM (SZD07001-2) for their financial support. We thank Prof. Ding Li for his help with the SHG measurements.

Supporting Information Available: X-ray crystallographic file in CIF format; simulated and experimental XRD patterns, and IR and UV−vis absorption spectra for the compound (PDF). This material is available free of charge via the Internet at http://pubs.acs.org.